ACS APPLIED MATERIALS & INTERFACES

Research Article

www.acsami.org

Investigation of Modified Graphene for Energy Storage Applications

Mohammad Arif Ishtiaque Shuvo, Md Ashiqur Rahaman Khan, Hasanul Karim, Philip Morton, Travis Wilson, and Yirong Lin*

Department of Mechanical Engineering, The University of Texas, El Paso, Texas 79968, United States

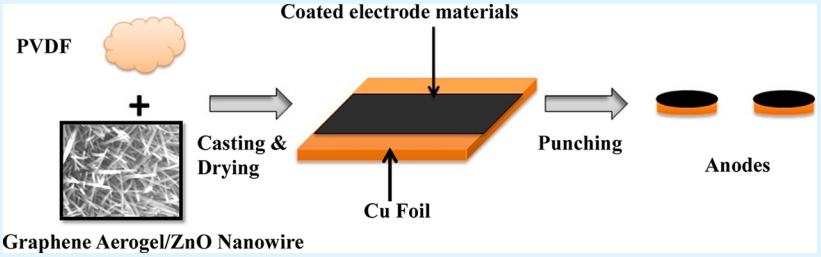

ABSTRACT: Lithium-ion batteries (LIB) have been receiving extensive attention because of the high specific energy density for wide applications such as electronic vehicles, commercial mobile electronics, and military applications. In LIB, graphite is the most commonly used anode material; however, lithium-ion intercalation in graphite is limited, hindering the battery charge rate and capacity. To overcome this obstacle, nanostructured anode assembly has been extensively studied to increase the lithium-ion diffusion rate. Among these approaches, high specific surface area metal oxide nanowires connecting nanostructured carbon materials accumulation have shown propitious results for enhanced lithium intercalation. Recently, nanowire/graphene hybrids were developed for the enhancement of LIB performance; however, almost all previous efforts employed nanowires on graphene in a random fashion, which limited lithium-ion diffusion rate. Therefore, we demonstrate a new approach by hydrothermally growing uniform nanowires on graphene aerogel to further improve the performance. This nanowire/graphene aerogel hybrid not only uses the high surface area of the graphene aerogel but also increases the specific surface area for electrode−electrolyte interaction. Therefore, this new nanowire/graphene aerogel hybrid anode material could enhance the specific capacity and charge−discharge rate. Scanning electron microscopy (SEM) and X-ray diffraction (XRD) are used for materials characterization. Battery analyzer and potentio-galvanostat are used for measuring the electrical performance of the battery. The testing results show that nanowire graphene hybrid anode gives significantly improved performance compared to graphene anode.

KEYWORDS: *graphene, lithium-ion battery, aerogel, nanowire*

1. INTRODUCTION

Electrochemical energy storage devices such as batteries and capacitors have been receiving great attention for electronic vehicles, cell phones, and other mobile electronic devices as energy sources. As a leading candidate among energy storage devices, lithium-ion-batteries (LIB) are in the highlighted area of research due to their lightweight and high specific energy.[15] Therefore, there is an increasing demand of research for developing potential LIB electrode materials with fast Li-ion diffusion, high electron transportability, and low resistance at the interface of electrode/electrolyte at high charge−discharge rates. Commercially, graphite is being used as the anode material for LIB which interacts (intercalation/deintercalation) with Li ions during the electrochemical process. A graphite anode accepts sufficient Li ions to form LiC_6 during charging as Li ions intercalate into the anode material and during discharging Li ions diffuse from the anode to the cathode. The extent to which this is carried out determines the specific energy density for the cell, therefore, amount of Li-ion diffusion is important for cell performance.[17] The multilayer nature of graphite materials limits Li-ion diffusion, resulting in low charge−discharge rate performance for the battery.

Graphene, a single layer of graphite with perfect 2D crystal of sp^2 hybridized carbon atoms, has been found to have extraordinary properties that can enhance LIB performance.[22] It has high specific surface area (2600 m^2/g) and can sustain at a current density up to six times that of copper.[5,16] It has also shown to have ballistic electron transportability with electron mobility as high as 15 000 $cm^2/(V\ s)$ and has incredible mechanical and thermal properties.[2,4,12] For having high specific surface area and excellent conductivity, graphene-based anode materials give room to Li ions in the anode for better diffusion, and thus enhanced battery performance was obtained. On the contrary, graphene sheets are prone to agglomeration because of van der Waals forces, which may form graphite again, thus hindering Li intercalation. Therefore, different metal oxides (Mn_3O_4, Fe_2O_3, Co_3O_4, etc.) had been grown on graphene sheets in the form of nanowires/nanoparticles to prevent agglomeration.[3,19,21,23] These grown nanoparticles enable graphene nanosheets of high conductive surface area leading to high electrode−electrolyte contact area

Received: May 23, 2013
Accepted: June 27, 2013
Published: June 27, 2013

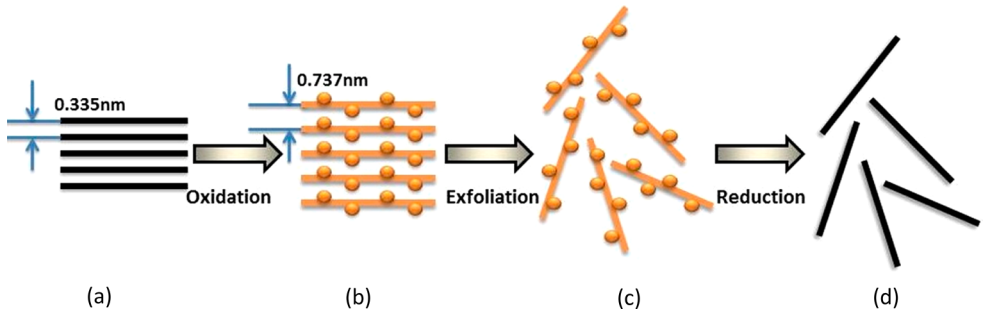

Figure 1. Graphene synthesis: (a) Natural graphite with inter layer spacing 3.34 Å. (b) Organic surface groups take place within the layers for oxidation and inter layer spacing becomes about 7.37 Å. (c) Graphite oxide solution is exfoliated by sonication and becomes dispersed graphene oxide solution. (d) Freeze-dried graphene oxide solution is reduced to graphene.[6].

and fast Li-ion diffusion rate. Previously, synthesis methods such as electrophoretic deposition, sol−gel, template-based method and hydrothermal growth have been developed for nanowire synthesis.[1,14,18] But in previous approaches, nanoparticles were distributed randomly in graphene sheets, which limits LIB performance.

Herein, we report a facile two-step hydrothermal method for growing uniformly distributed aligned ZnO nanowires (ZnO NWs) on graphene aerogel for LIB electrodes, compared with bare graphene electrode. ZnO in various structures have shown high reversible capacity and rate capacity when used in LIB as anode materials.[10] Moreover, to the best of our knowledge, anode material with aligned ZnO NWs has not yet been reported. A low temperature hydrothermal method was used for growing these aligned nanowire arrays with open space which allows easy diffusion of Li ions into the inner region of electrode, resulting in improved energy density and performance. Also, because each nanowire is vertically grown on the substrate, it is directly contacted with the current collector substrate and each nanowire could participate in energy conversion process, resulting in significantly increased charge and discharge rates for LIB upon future investigation.

2. EXPERIMENTAL DETAILS

2.1. Graphene Aerogel Synthesis. Crystalline graphite powder (325 mesh, 99%, Alfa Aesar) was used in graphene synthesis by Hummer's method with additional $KMnO_4$.[11] Three grams of graphite and 1.5 g of sodium nitrate ($NaNO_3$, Alfa Aesar) were mixed with 69 mL of sulphuric acid (Fisher) using an ice bath. Later 9 g of potassium permanganate $KMnO_4$ (Alfa Aesar) was added to the solution. Next the solution beaker was transferred into a water bath where the solution was heated with stirring at 35 °C for 7 h. After that an additional 9 g of $KMnO_4$ was added and again heated at 35 °C for 12 h. Later the solution was poured into 400 mL of ice containing 3 mL o fH_2O_2. Next, the solution was centrifuged for 30 min at 4000 rpm and the supernatant was decanted away. Obtained solid material was washed by water, 30% HCl and Ethanol (3 times) successively. Every time after washing, the solution was sifted, centrifuged (4000 rpm, 3 min) and the supernatant were decanted away. The remaining solid material was dried overnight in a desiccator. A solution of 30 mg/mL was produced and sonicated (1 h bath and 5 min tip sonicated). Next the solution was freeze-dried and graphene oxide aerogel (GOA) was obtained. In order to obtain graphene aerogel (GA) we reduced the GOA. The GOA was thermally reduced in an argon atmosphere at 1050 °C for 5 min with temperature ramp of 1 °C/min up to 300 °C followed by ramp of 20 to 1000 °C. Excessively high ramp rates can cause deflagration of the material. The GA fabrication process is schematically shown in Figure 1.

2.2. Graphene/Zinc Oxide Nanowire Hybrid Synthesis. The ZnO nanowire growth is a two-step hydrothermal growth method including seeding and nanowire growth. Briefly, ZnO nanoparticle seeds were first synthesized in an organic solution, and then the seeding process was performed to coat ZnO nanoparticles onto graphene aerogel. Those seeded graphene aerogels were transferred to ZnO nanowire hydrothermal growth solution at elevated temperature and atmosphere pressure. After the nanowire growth, the nanowire/graphene aerogel were rinsed extensively and dried in air for LIB anode fabrication.

ZnO Seed Particles. A 12.5 mM zinc acetate (98.0% purity, Sigma Aldrich) dehydrate ethanol solution was prepared at 50 °C under vigorous stirring.[8] After completely dissolved, the solution was cooled down to room temperature and diluted to a concentration of 1.4 mM by adding extra ethanol. Twenty millimoles of sodium hydroxide (Acros) ethanol solution was prepared at 60 °C under vigorous stirring and cooled to room temperature, additional ethanol was added in order to dilute to 5.7 mM. These two solutions were mixed at a volume ratio of 18:7 at a temperature of 55 °C for 30 min to form ZnO nanoparticle seeds. The reactions involved in formation ZnO seed particles are as follows

$$Zn^{2+} + 2OH^- \leftrightarrow Zn(OH)_2$$

$$Zn^{2+} + 2OH^- \leftrightarrow Zn(OH)_2Zn(OH)_2 + 2OH^- \leftrightarrow [Zn(OH)_4]^{2-}$$

$$[Zn(OH)_4]^{2-} \leftrightarrow ZnO_2 + 2H_2O$$

$$ZnO_2^{2-} + H_2O \leftrightarrow ZnO + 2OH^-$$

$$ZnO + OH^- \leftrightarrow ZnOOH^-$$

ZnO Nanowires. The first step of the nanowire growth is seeding process. GA was dipped in the seed solution for 5 min and subsequently annealed on a hot plate at 150 °C for 10 min to enhance adhesion between the GA and nanoparticles. Hydrothermal growth of ZnO nanowires was performed using a low temperature hydrothermal method detailed elsewhere.[4] Briefly, an aqueous solution of 25 mM zinc nitrate hexahydrate ($Zn(NO_3)_2{\cdot}6H_2O$, 99.9% purity, Sigma-Aldrich), 25 mM hexamethylenetetramine (HMTA) ($C_6H_{12}N_4$, 99.9% purity, Sigma-Aldrich), and 5−7 mM polyethylenemine (PEI, Branched) were prepared at room temperature. GAs were immerged in growth solution when the temperature was at 85 °C. The time duration of this growth was 2 h for all the GA samples. After the reaction had been completed, GA samples were taken out of the solution and rinsed with deionized water and dried at 100 °C on a hot plate for 2 h. Chemical reactions involved in formation of ZnO nanowires are as follows

$$HMTA + 6H_2O \leftrightarrow 4NH_3 + 4HCHO$$

$$NH_3 + H_2O \leftrightarrow NH_4^+ + OH^-$$

$$Zn^{2+} + 2OH^- \leftrightarrow Zn(OH)_2$$

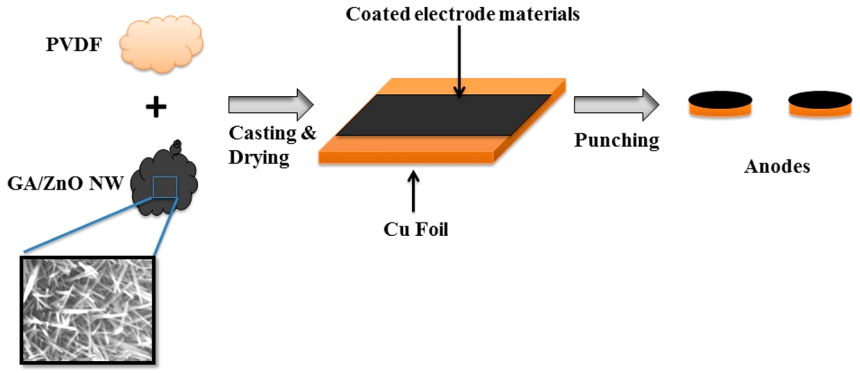

Figure 2. Schematic view of anode preparation.

$$Zn(OH)_2 \leftrightarrow ZnO + H_2O$$

2.3. Anode Preparation. For making both graphene and ZnO NW-coated graphene anodes, polyvinylidene fluoride (PVDF, MTI corp., purity ≥99.5%, molecular weight 600 000) was used as binding material. PVDF was dissolved in N-Methyl-2-pyrrolidone (NMP, MTI corp., purity ≥99.5%) at a 1:10 weight ratio by heating at 80 °C. A slurry of 90 wt % graphene and 10 wt % PVDF was made using PVDF-NMP solution. For ZnO NWs/graphene, 80:20 wt % ratios was used with PVDF. Excess NMP was used to ease the mixing of slurry. Both horn and bath sonication were used to make a homogeneous mixture. The slurry was casted on copper foil and subsequently dried overnight at 120 °C. A precision disc cutter from MTI Corporation was used to cut anodes with 12 mm diameter. The anode preparation process is schematically shown in Figure 2.

2.4. Coin Cell Assembly. Coin cells (CR 2032) were assembled using either bare graphene anode or ZnO NW arrays/graphene anode. Each of the anodes was investigated against 12 mm diameter single-side $LiCoO_2$ coated on Al foil as cathode (MTI corp., 0.1 mm thickness). One molar $LiPF_6$ in ethylene carbonate (EC), dimethyl carbonate (DMC), and diethyl carbonate (DEC) organic solvent at 1:1:1 volume ratio was used as electrolyte as received (MTI corp.). All the batteries were made inside of argon-filled (purity 99.999%) glovebox (LABstar, MBraun) where oxygen and moisture content were kept less than 0.01 ppm. A cross-sectional view for coin cell assembly is shown in Figure 3.

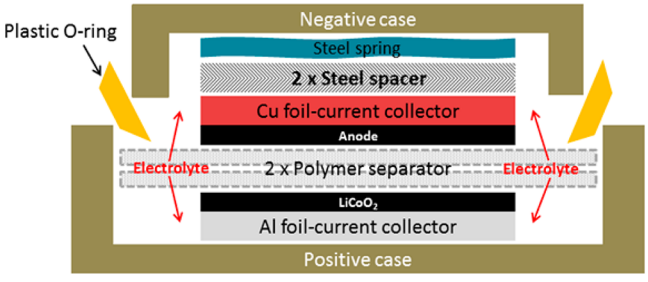

Figure 3. Cross-sectional view of coin cell assembly.

3. RESULTS AND DISCUSSION

The surface morphology of GA and GA with ZnO nanowire is shown in Figure 4. Wrinkled topography of GA with high surface area can be understood from the low- and high-magnification images (Figure 4a, b). The pore size of the thermally reduced virgin GA is approximately 5−20 μm, as estimated from the images. Note that all of the GA samples shown in Figure 4 were freeze-dried from GO aqueous solution with a concentration of 30 mg/mL. The single layer nature of the synthesized graphene was demonstrated previously thus will not be discussed here.[9] As indicated by Figure 4c, d, ZnO nanowires are grown uniformly throughout the GA with an average diameter of 30 nm and length of 1 μm. Because of the wavy nature of GA, ZnO nanowires growth followed its surface topography, indicating the aerogel morphology was maintained after the nanowire growth. This is also validated by the evidence that the shape and volume of GAs before and after nanowire growth did not change.

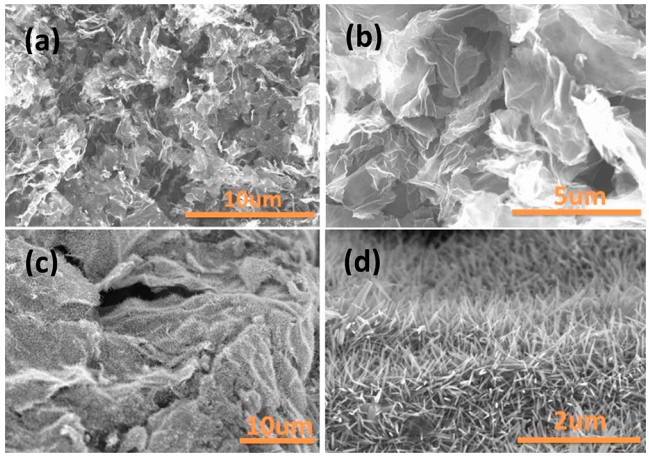

Figure 4. SEM images: (a, b) graphene aerogel, (c, d) graphene aerogel with ZnO nanowire.

XRD patterns were obtained to confirm the crystal structures of GA and nanowires (see Figure 5). After the freeze-drying process, graphene oxide contains water molecules along with

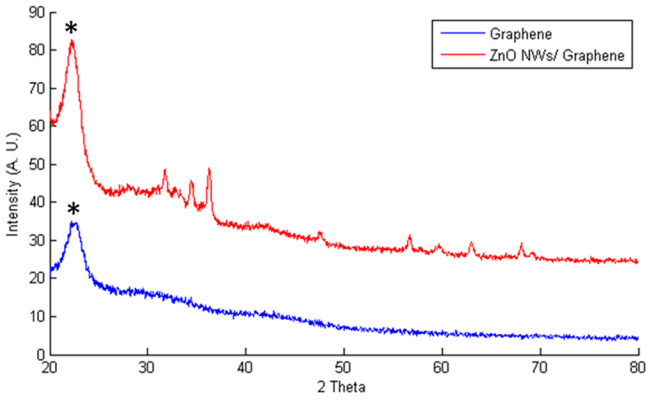

Figure 5. XRD results for graphene and ZnO NWs/graphene. Asterisk (*) peak is for graphene. The rest of the peaks belong to ZnO.

dx.doi.org/10.1021/am401978t | ACS Appl. Mater. Interfaces 2013, 5, 7881−7885

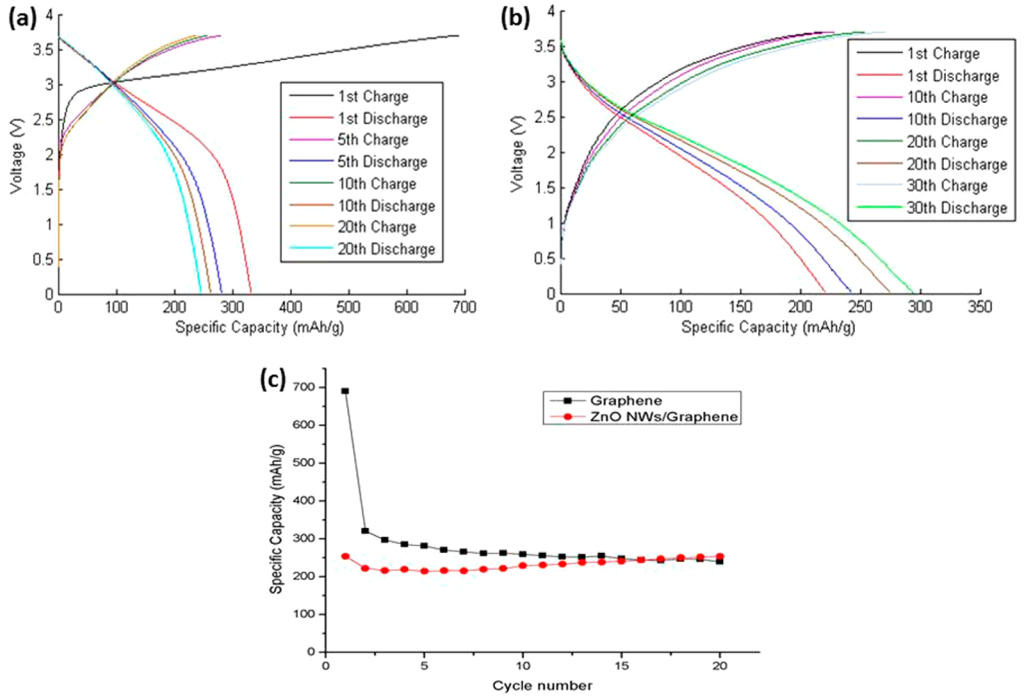

Figure 6. Measurements of capacity and rate capability. (a) Carge/discharge curve for GA anodes,(b) charge/discharge curve for GA with ZnO nanowires anode,(c) comparison of specific capacity of the two anode materials as a function of cycle number.

some surface functional groups (−OH, −COOH etc.).[13] During reduction of graphene oxide, it loses water molecules upon heating to 200 °C and gets fully rid of the functional group by heating up to 1000 °C. As graphene has 2D crystal structure, there should not be any XRD peak for graphene. However, during the freeze-drying and thermal reduction process, the exfoliated GO sheets are thermodynamically instable; they tend to stack with each other for a more stable state. The peak of GA at around 23 degrees showed the evidence of this stacking phenomenon.

Unlike the thermally reduced graphene sample reported elsewhere, the 2θ peak of graphene typically has value of 26θ; the 2θ peak of the GA studied here is around 22°, indicating a large space in between the sheets. This is because the graphene is synthesized from freeze-drying, where the morphology and spacing between graphene sheets are maintained after thermal reducing. Typically, graphene is reduced from graphene oxide power, where the graphene is free to stacking back to each other after the water vapor and surface functional groups are removed. The enhanced spacing between graphene sheets could benefit the lithium ion diffusion, leading to better charge and discharge capability in LIB. Note the GA/ZnO also showed peaks belong to ZnO, all peaks match the standard card of these materials, and no peaks from impurity phase were shown.

Two types of LIBs were prepared with GA and GA with ZnO nanowires as working electrode, respectively. To evaluate the electrochemical performance of the anodes, we used an eight-channel battery analyzer from MTI Corporation. Figure 6 shows galvanostatic charge discharge curves for the two kinds of working electrode and cycle performance comparison between the two kinds of anodes. For both cases, $LiCoO_2$ cathode was used as counter electrode. Panels a and b in Figure 6 show galvanostatic charge−discharge curves for GA and GA with ZnO nanowire anodes, respectively, at current density 100 mA/g and voltage window between 0.01 to 3.7 V in the first, fifth, 10th, and 20th cycles. Note that no obvious voltage plateau was observed for both cases. The first charge capacity of graphene anode (690 mA h/g) is way higher than that of GA/ZnO NW anode (249 mA h/g), and the same trend was found in discharge capacity. With the increase in cycle numbers lithium storage performance of GA anode drops. Coulombic efficiency of GA/ZnO NW electrode was always found above 98%, and its lithium storage performance increased with the increase in cycles. The 20th discharge−charge capacities are 245 and 240 mA h/g for GA, 298 and 295 mA h/g for GA/ZnO NW electrode. The GA anode loses its reversibility where the GA/ZnO NW anode gains reversibility with cycle numbers. More importantly, the GA/ZnO NW anode exhibits a much better cycling performance than the GA anode (Figure 6c). It can be seen that the reversible capacity of GA decreases from 690 to 245 mA h/g up to 20 cycles. On the contrary, the capacity of the GA/ZnO NW electrode was around 249 mA h/g after the first cycle, which falls slightly after that and then gradually increases and goes above the GA anode's capacity with time. Obviously, this is due to the ZnO nanowires, because all other assembling parameters for both the batteries were same and same testing parameter is used. It can be explained this way that charge discharge cycles create more space for better Li-ion diffusion, augmenting the specific capacitance in GA/ZnO NW as the cycle number increases. Therefore, there is an excellent synergistic effect between ZnO nanowires and graphene aerogel in the anode that becomes more acute with cycles and performs a vital play in the excellent cycling performance of GA/ZnO NW anode. Lower capacity in the beginning resulted from the incomplete reaction and irreversible lithium loss because of the formation of solid electrolyte interface (SEI) layer.

The obtained result indicates that aligned ZnO nanowires on graphene aerogel provide better properties, i.e., capacity, Coulombic efficiency, rate capability and cycling stability for LIB than GA. Reasons for the improved performance of the developed GA/ZnO NW anode material can be a few. First,

aligned nanowires between graphene sheets prevent the graphene sheets from agglomerating, preserving high surface area which is favorable for Li-ion storage. Second, graphene has good electrical conductivity which benefits the anode in achieving low resistance and electronic/ionic conductivity, therefore leading to a higher specific capacity.[7,20] Third, GA/ZnO nanowires provide elastic buffer space for Li-ion during intercalation/deintercalation, which prevents cracking or crumbling of the anodes retaining the original properties. Finally, GA/ZnO NW anode provides large electrode/electrolyte contact area and short path length for Li-ion diffusion with good stability, thus maximize the Li-ion transport. The above-mentioned reasons are expected to be responsible for the improved anodes with excellent energy storage capacity, cycling stability, and Coulombic efficiency.

4. CONCLUSION

In summary, energy storage devices such as battery and super capacitor are receiving increasing attention because of their high specific energy density and fast charge and discharge capability. A low-temperature hydrothermal method has been utilized to synthesize GA/ZnO NW for high performance LIB anode, whereas graphene aerogel was synthesized by freeze-drying method. SEM image demonstrated that the porous structure was maintained after thermal reduction and nanowires are uniformly distributed on the aerogel surface. XRD analysis showed that the spacing between the graphene sheets is higher than reduced graphene powder because of the morphology of the aerogel. Excellent performance was found from GA/ZnO NW anode compared to GA anode in terms of capacitance and cycle stability. The growth of nanowires has a positive synergistic effect which prevents graphene agglomeration and provides pathways for better Li-ion diffusion incrementing electrode−electrolyte contact area. This simple method can be utilized commercially for making high-performance anodes for LIBs.

AUTHOR INFORMATION

Corresponding Author

*E-mail: ylin3@utep.edu. Tel: (915)-747-6015.

Notes

The authors declare no competing financial interest.

REFERENCES

(1) Arico, A. S.; Bruce, P.; Scrosati, B.; Tarascon, J. M.; Schalkwijk, W. V. *Nat. Mater.* **2005**, *4*, 366−77.
(2) Balandin, A. A. *Nat. Mater.* **2011**, *10*, 569−81.
(3) Chen, S. Q.; Wang, Y. *J. Mater. Chem.* **2010**, *20*, 9735−39.
(4) Fang, Y.; Guo, S.; Zhu, C.; Zhai, Y.; Wang, E. *Langmuir* **2010**, *26*, 11277−82.
(5) Geim, A. K. *Science* **2009**, *324*, 1530−34.
(6) Jeong, H. K.; Lee, Y. P.; Lahaye, R. J. W. E.; Park, M. H.; An, K. H.; Kim, I. J.; Yang, C. W.; Park, C. Y.; Ruoff, R. S.; Lee, Y. H. *J. Am. Chem. Soc.* **2008**, *130*, 1362−66.
(7) Jiang, C.; Hosono, E.; Zhou, H. *Nano Today* **2006**, *1*, 28−33.
(8) Lin, Y.; Ehlert, G.; Sodano, H. A. *Adv. Funct. Mater.* **2009**, *19*, 2654−60.
(9) Lin, Y.; Ehlert, G. J.; Bukowsky, C.; Sodano, H. A. *ACS Appl. Mater. Interfaces* **2011**, *3*, 2200−03.
(10) Liu, J.; Li, Y.; Ding, R.; Jiang, J.; Hu, Y.; Ji, X.; Chi, Q.; Zhu, Z.; Huang, X. *J. Phys. Chem. C* **2009**, *113*, 5336−39.
(11) Marcano, D. C.; Kosynkin, D. V.; Berlin, J. M.; Sinitskii, A.; Sun, Z.; Slesarev, A.; Alemany, L. B.; Lu, W.; Tour, J. M. *ACS Nano* **2010**, *4*, 4806.
(12) Meyer, J. C.; Geim, A. K.; Katsnelson, M. I.; Novoselov, K. S.; Booth, T. J.; Roth, S. *Nature* **2007**, *446*, 60−63.
(13) Moon, I. K.; Lee, J.; Ruoff, R. S.; Lee, H. *Nat.Commun.* **2010**, *1*, 73.
(14) Sakamoto, J. S.; Dunn, B. *J. Mater. Chem.* **2002**, *12*, 2859−61.
(15) Scrosati, B. *Electrochim. Acta* **2000**, *45*, 2461−66.
(16) Si, Y.; Samulski, E. T. *Chem. Mater.* **2008**, *20*, 6792−97.
(17) Wakihara, M. *Mater. Sci. Eng.,R* **2001**, *33*, 109−34.
(18) Wang, D.; Choi, D.; Li, J.; Yang, Z.; Nie, Z.; Kou, R.; Hu, D.; Wang, C.; Saraf, L. V.; Zhang, J. *ACS Nano* **2009**, *3*, 907−14.
(19) Wang, H.; Cui, L. F.; Yang, Y.; Casalongue, H. S.; Robinson, J. T.; Liang, Y.; Cui, Y.; Dai, H. *J. Am. Chem. Soc.* **2010**, *132*, 13978−80.
(20) Wu, Z. S.; Ren, W.; Gao, L.; Liu, B.; Jiang, C.; Cheng, H. M. *Carbon* **2009**, *47*, 493−99.
(21) Wu, Z. S.; Ren, W.; Wen, L.; Gao, L.; Zhao, J.; Chen, Z.; Zhou, G.; Li, F.; Cheng, H. M. *ACS Nano* **2010**, *4*, 3187−94.
(22) Yoo, E. J.; Kim, J.; Hosono, E.; Zhou, H.; Kudo, T.; Honma, I. *Nano Lett.* **2008**, *8*, 2277−82.
(23) Zhou, G.; Wang, D. W.; Li, F.; Zhang, L.; Li, N.; Wu, Z. S.; Wen, L.; Lu, G. Q.; Cheng, H. M. *Chem. Mater.* **2010**, *22*, 5306−13.